Renewable Energy 256 (2026) 124668

Contents lists available at ScienceDirect

Renewable Energy

journal homepage: www.elsevier.com/locate/renene

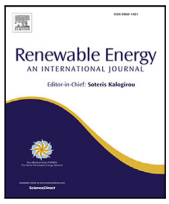

Tidal and wave driven hydrokinetic power in atolls of an amphidromic region in the Pacific Ocean

Federico Zilic de Arcos [a,b,*], Minh Anh Pham [a], Franck Lucas [c], Marc Lafosse [d], Grégory Pinon [a,**]

[a] Laboratoire Ondes et Milieux Complexes - Normandie Univ, UNIHAVRE, CNRS, 53 rue Prony, Le Havre, 76600, Normandy, France
[b] Department of Engineering Science, University of Oxford, Parks Road, Oxford, OX1 3PJ, United Kingdom
[c] GEPASUD, University of French Polynesia, Faa'a, French Polynesia
[d] Energie de la Lune, 87 Quai des Queyries, Bordeaux, 33100, France

ARTICLE INFO

Keywords:
Tidal energy
Tidal currents
Wave energy
Overtopping
Atolls

ABSTRACT

French Polynesia is located in an amphidromic area of the Pacific Ocean, a region of low tidal ranges. Atolls, ring-shaped islands with internal lagoons that are common to this region, often show strong currents in channels that connect their lagoon to the ocean. This study shows long-term in-situ flow measurements using acoustic-Doppler current profilers that were deployed in the main channels of Manihi and Takaroa, two atolls of French Polynesia, to explore their kinetic energy potential. Despite the low tidal effects on sea levels, flow measurements show strong currents with a semidiurnal behaviour dominated by the lunar constituent. An asymmetry in the ebb and flood currents is observed, and correlation with wave climate indicate that the atolls operate as large wave overtopping devices, increasing the kinetic energy flux through the channel, and extending the ebb flow period. An energetic assessment shows a potential for tidal stream turbines to produce a substantial proportion of the energy demands of Manihi and Takaroa. This energy production would likely have a limited environmental and visual impact, and would allow for a reduction in carbon emissions and reliance on fossil fuels.

1. Introduction

French Polynesia, as well as other small island states in the Pacific, depend on imported hydrocarbons for energy production [1,2]. In 2019, petroleum-based fuels accounted for 94% of the energy consumed in French Polynesia. This includes the inhabitants' consumption, transport and tourism-related activities such as resort operation. Energy production based on fossil fuels harms their main source of activity: the environmental splendour of the archipelago.

The public sector and civil society have pushed for the diversification of the energy matrix in French Polynesia and the adoption of renewable energy sources. Between 2015 and 2020, the penetration of renewable energy in the electricity grid increased. By 2020, the islands had approximately 30% of their total electric power capacity coming from renewables, mainly through the implementation of hydro and solar power plants [3]. The figure, however, hides disparities across the archipelago. While some of the islands, newer in geological terms, are formed by large mountains with geographic features that are suitable for hydropower, older islands of low elevation and at the stage of atolls are not suited for this form of energy. Atolls, then, rely more heavily on fossil fuels than mountainous islands.

The Polynesian authorities have set targets to generate 75% of their electricity from renewable sources by 2030, launching an ambitious Energy Transition Plan (ETP) with a support programme set by the *Agence Française de Développement* (AFD) and the Polynesian Government [4]. Ocean energy is one of the energy resources considered, given the hundreds of islands and atolls that compose French Polynesia and that stretch over more than 2000 kilometres in the South Pacific Ocean [5]. The area covered by French Polynesia is comparable to the entire European continent, albeit with a population in the order of 300,000 inhabitants. Sustainable power generation strategies need to account for the challenges and limitations of such an environment, with special consideration for isolated islands and small communities.

Large-scale wind and solar power are the backbone of current decarbonisation efforts worldwide. Their applicability in French Polynesia, however, is challenged due to their visual impact likely to

* Corresponding author at: Department of Engineering Science, University of Oxford, Parks Road, Oxford, OX1 3PJ, United Kingdom.
** Corresponding author.
E-mail addresses: federico.zilic@eng.ox.ac.uk (F. Zilic de Arcos), gregory.pinon@univ-lehavre.fr (G. Pinon).

https://doi.org/10.1016/j.renene.2025.124668
Received 16 June 2025; Received in revised form 19 October 2025; Accepted 24 October 2025
Available online 30 October 2025

affect tourism, the main activity in the islands, as well as due to their intermittent nature. Other alternatives are thus being explored.

Wave energy is abundant and evenly distributed across the numerous islands [6], but despite resource availability, the cost of wave energy conversion technologies remains high compared to other alternatives [7]. The geographical characteristics of French Polynesian islands also suggest the need for device adaptation to local conditions. A typical atoll is composed of a low-depth lagoon, one or more passes connecting the lagoon with the ocean, a coral reef surrounding the lagoon, and a steep decline of the seabed outside the atoll, reaching depths up to 1000 m near the shoreline [8]. This presents challenges not only to logistics but also to finding suitable solutions for anchoring wave energy devices. Current efforts, such as the Tahiti Wave Energy Challenge (TWEC), which aimed at promoting the development of wave energy in conjunction with the 2024 Olympic surfing competition in Tahiti, could become a turning point [9]. However, at the time of writing, wave energy does not yet appear as a viable alternative.

Typical bathymetric conditions are favourable for Ocean Thermal Energy, either for Sea-Water Air-Conditioning (SWAC) or for electricity generation. Three SWAC installations with capacities in the order of a few MW exist to date [8], but the level of technological development is still limited for both SWAC and electricity generation, and no commercially viable alternatives exist yet in the market [8,10].

Tide-driven currents, where available, are an alternative to supply renewable power to small grids due to their predictability [11]. Local fishermen and sailors in French Polynesia often report strong currents within the atolls, and Lewis et al. [12] suggested that coral reefs could also act as natural infrastructure for wave overtopping, where hydrokinetic turbines could convert wave-driven currents flowing through atoll channels. Neither of these hypotheses, however, has yet been confirmed by *in situ* flow measurements, and ocean hydrokinetic energy has often been disregarded in French Polynesia due to the region's low tidal amplitudes [2].

Marine energy standards describe protocols for flow measurement in order to assess the feasibility of tidal stream energy converters, estimating annual energy production of single devices, and for validating and calibrating numerical models required for the design of tidal turbine arrays [13]. Acoustic Doppler Current Profilers (ADCP) are the industry standard tool to perform on site flow measurements across different depths and typically over long periods of time.

ADCPs have been widely used to characterise sites of interest for the development of tidal stream energy. Sellar et al. [14] performed detailed current speed measurements at the European Marine Energy Centre EMEC (Orkneys, Scotland). Cossu et al. [15] performed measurements to characterise the Banks Strait (Tasmania, Australia) as a potential site for tidal stream energy development. Neill et al. [16] used ADCP measurements to characterise the Marine Energy Test Area (META) in Wales. Evans et al. [17], using ADCPs to study the tidal currents at EMEC, discussed the IEC standards [13] and generally agreed with the industrial recommendations. Lewis et al. [18] used ADCP measurements to determine generic power law flow profiles that could be used by turbine designers. They found that a 1/7th power law profile with a 0.4 roughness coefficient describes the mean velocity profiles at two sites in the Irish sea. Long term current and tide measurements are also critical for validating hydrodynamic models which can then be employed to predict the flow field across wider geographical areas, a necessary step for farm layout design. Some examples include the work of Guerra et al. [19] and Suarez et al. [20], who sampled and modelled the Chacao channel and the Magellan Strait, respectively, both located in Chile; and the work of Yang et al. [21], which shows a hydrodynamic model of the Salish Sea, Canada, validated against an extensive suite of ADCP measurements.

The Service of Energy of the French Polynesia Government, as part of their energy transition strategy, commissioned exploratory current-velocity measurements at two passes: Tairapa and Teauonae, located at the Manihi and Takaroa atolls, respectively. The two campaigns were conducted for approximately one year mainly using bottom-mounted ADCPs, with the deployment location informed by a preliminary survey conducted from a boat [22]. No similar campaigns in atoll channels have been executed to the best of the authors' knowledge. The instruments were deployed and used to measure velocity vectors at different depths across the water column, with measurements averaged over five minute periods.

This paper presents an analysis of the current-velocity measurements at both sites to assess their viability for energy production. The objective is to present an initial assessment of the available resource, and to compare the potential for energy generation with the local power consumption. The results showed a promising kinetic energy flux through both channels driven by a strong tidal influence with contributions from wave overtopping.

The paper is organised as follows: It starts with a general description of the two analysed sites, followed by the measurement and processing techniques in Section 2.2. An analysis of the data is presented in Section 3 with Section 4 detailing the potential for hydrokinetic energy production. The conclusions are finally presented in Section 5.

2. Site description and methods

French Polynesia is composed by five archipelagos: *îles de la Société, îles Tuamotu, îles Gambier, îles Australes* and *îles Marquises*, with around 2000 kilometres from north to south and from east to west. The 5 archipelagos contain approximately 120 islands and cover a combined maritime and terrestrial area slightly larger than the surface of Europe.

The total population of French Polynesia is nearly 300,000 inhabitants. Tahiti, the main island, concentrates approximately 200,000 people, while remote islands, often located hundreds of kilometres away from Tahiti, can often have populations in the order of tens of inhabitants.

Manihi and Takaroa are two atolls located in the Tuamotu Archipelago. These are ring-shaped islands, with a thin strip of land and coral reefs enclose a lagoon in the middle. Each atoll has at a main pass connecting the lagoon with the open ocean. The channels at Manihi and Takaroa are named Tairapa (Fig. 2) and Teauonae (Fig. 3), respectively.

Most of French Polynesia is located at an amphidromic region, an area of the sea where the amplitude of tidal lunar constituents is low. This typically results in small tidal amplitudes, as shown in Fig. 1, and potentially with a preponderance of solar influence. However, small tidal amplitudes are not necessarily correlated with slow currents, as these can be driven by tides outside of the amphidromic region, as well as by other local phenomena.

2.1. Manihi

Satellite pictures of Tairapa, Manihi's channel, are shown in Fig. 2. The channel is oriented at approximately 45° from the north. The cross-section of the channel is approximately 80–100 m wide and about 6.5 m deep. The seabed of Tairapa is composed of sand and coral residuals. The channel is frequently transited by small crafts, as this is the only suitable marine access to the lagoon. Local reports also suggest frequent use of the channel by endemic fauna, including fish, sharks, and marine mammals. A diagram of the channel's cross section, produced using depth readings from the preliminary survey that informed ADCP location, is presented in Fig. 4.

The bottom-fixed ADCP was deployed at [14°27,324″ S; 146°03,529″ W; WGS84]. The sensor was placed in the channel, close to the inner boundary of the atoll, and next to the northern edge of the channel. The deployment location of the ADCP is shown in the right picture of Fig. 2.

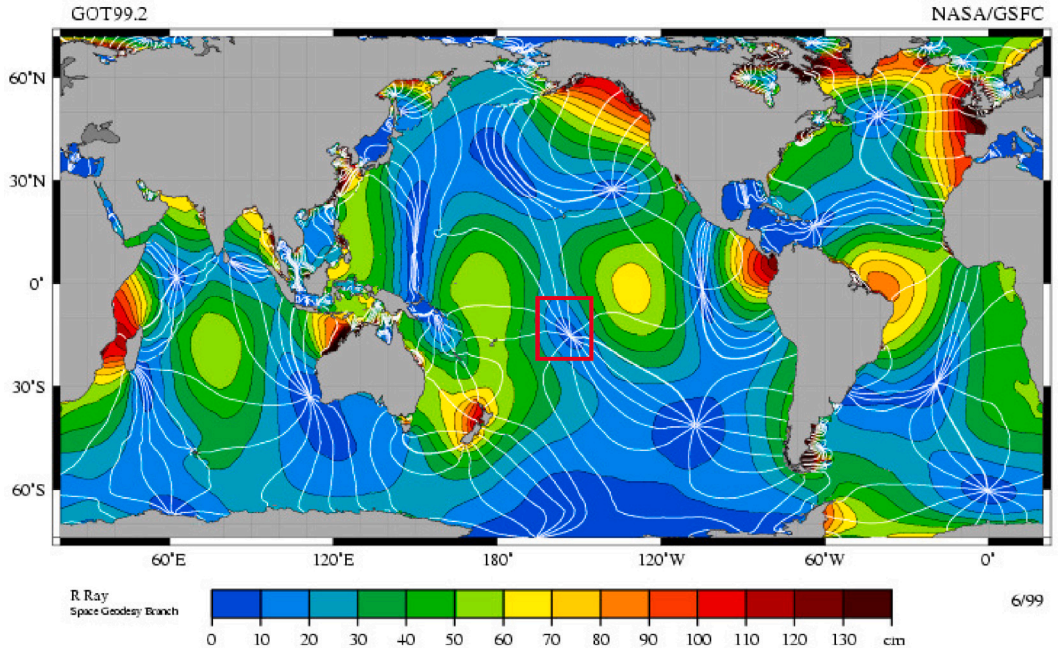

Fig. 1. Global patterns of amplitude of the principal lunar semidiurnal constituent of tides. Overlay of red rectangle marks the amphidromic region of French Polynesia.
Source: NASA figure reproduced from [23].

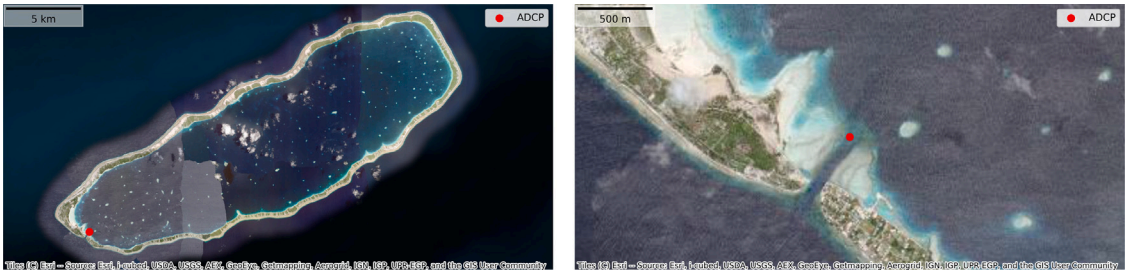

Fig. 2. Satellite picture of Manihi (left) and zoom on the Tairapa channel (right). Red markers highlight the location of ADCP deployment. Map images are the intellectual property of Esri and are used herein under license.

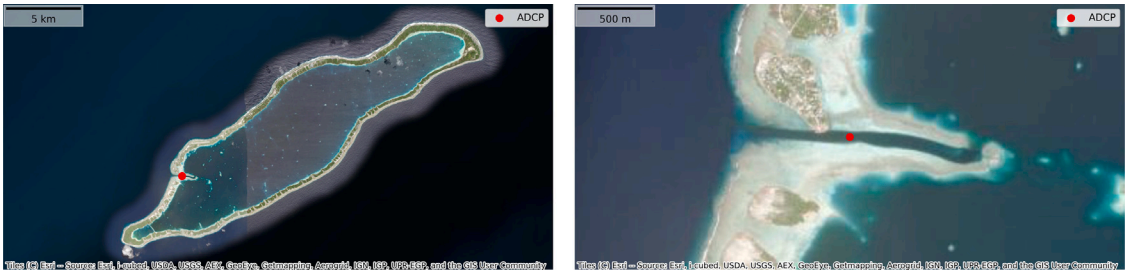

Fig. 3. Satellite picture of Takaroa (left) and zoom on the Teauonae channel (right). Red markers highlight the location of ADCP deployment. Map images are the intellectual property of Esri and are used herein under license.

2.2. Takaroa

Satellite pictures of Teauonae, Takaroa's main channel, are shown in Fig. 3. The cross-section of the channel is approximately 60–70 m wide and approximately 16–17 m deep. The channel is oriented at nearly 90° from the north. Fig. 4 shows a diagram of Teauonae's cross section.

The site for the ADCP deployment was located at [14°28,519″S; 146°02,132″W; WGS84] (Fig. 3). The spot is near the centre of the channel, and close to the border of the internal lagoon. The deployment location had a depth of 16.5 m. The seabed of this channel is also composed of sand and coral residuals, and is regularly used by small crafts and endemic fauna.

2.3. Measurement techniques

Tairapa and Teauonae were surveyed in two stages. The first was a preliminary campaign using a boat-mounted ADCP to identify promising zones in each channel for long-term sensor placement [24]. The raw data of this campaign were not available to this study. Once the zones of interest were identified, up-looking bottom-fixed ADCPs were deployed

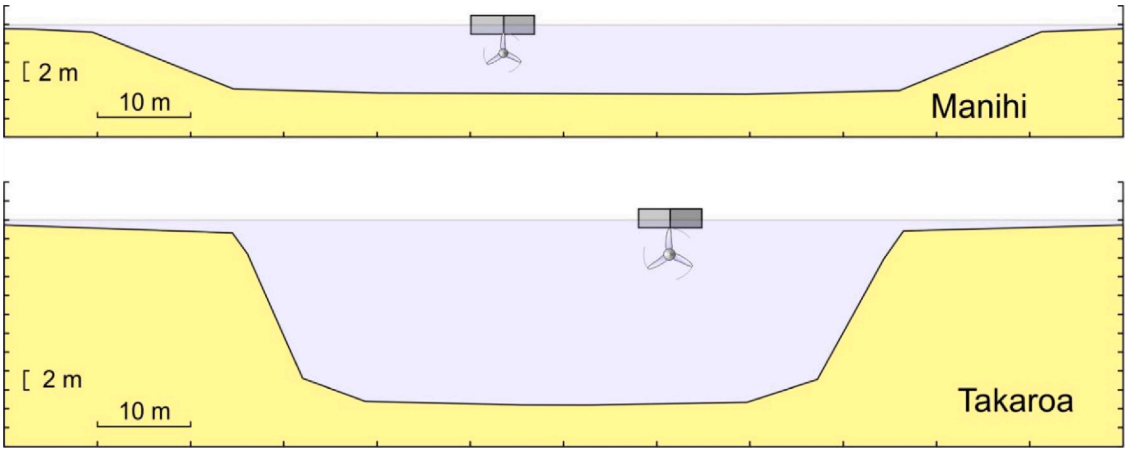

Fig. 4. Cross-sectional area sketches of both channels. Small-scale floating turbines near the surface.

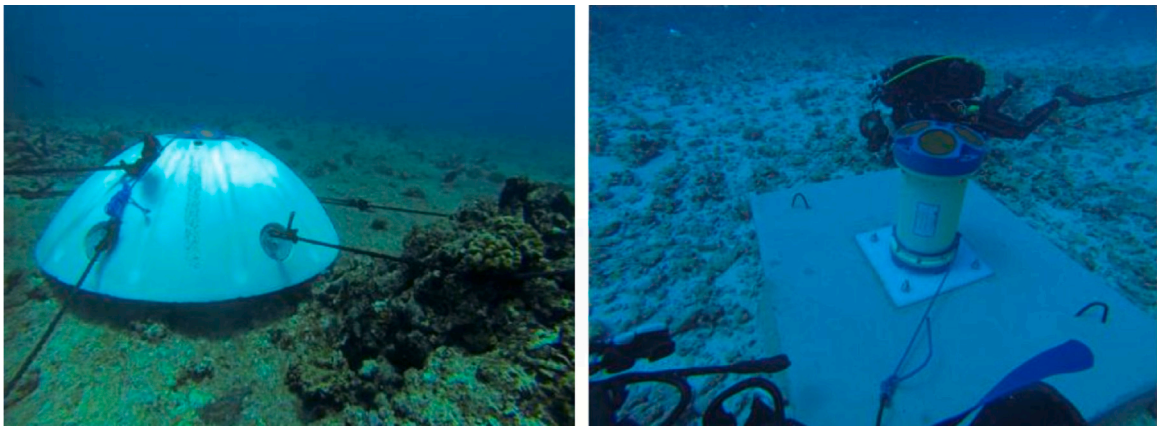

Fig. 5. Pictures of the ADCP deployments at Manihi (left) and Takaroa (right).

for just over a year to measure the evolution of current speed and direction across the water column. Two 4-beam RDI Workhorse sentinel 600 kHz, manufactured by Teledyne, were installed, as shown in Fig. 5. Each ADCP included a pressure sensor to measure water column height and detect free surface variations through the campaign. Measurements were taken every 5 min and were composed of 40 pings at 7.5 s intervals, providing velocity profiles with 0.5 m vertical bins starting 1.63 m above the transducer. These bottom-fixed measurements are presented and discussed below.

Quality control of ADCP data followed manufacturer guidelines. Each 5 min ensemble averaged 40 pings, with internal filters applied through RDI commands: WA 090 (rejects false targets by limiting beam-to-beam echo-intensity differences), WC 064 (discards velocity data with correlation below 64 counts), and WE 4000 (sets a maximum allowable error velocity of 4 m/s, effectively disabling the filter to retain all valid data). This was done to exclude spurious or low-quality returns. Pitch and roll were checked and remained within the manufacturer threshold of ± 15 ° throughout the campaign at both sites. Finally, the upper ≈6% of bins were removed to avoid surface echo contamination.

Campaign length was 396 days and 406 days for Manihi and Takaroa, respectively. The campaigns took place between December 2015 and January 2017. Data were recovered four times during these intervals, as described in Table 1.

Table 1
Dates of ADCP deployment and data recovery for the studied sites.

Event	Manihi		Takaroa	
	Date	Days	Date	Days
Deployment Recovery	09/12/2015 14/03/2016	96	15/12/2015 28/03/2016	104
Deployment Recovery	27/03/2016 15/07/2016	110	28/03/2016 16/07/2016	110
Deployment Recovery	15/07/2016 03/10/2016	81	16/07/2016 04/10/2016	81
Deployment Recovery	03/10/2016 20/01/2017	109	04/10/2016 23/01/2017	111
Total duration		**396**		**406**

3. Measured data analysis

3.1. Surface elevation

Fig. 6 shows sample time series and corresponding Fast Fourier Transforms (FFTs) of surface elevation computed from the ADCPs' pressure sensors. Sample series are plotted across a period of 14 days to capture spring and neap tides.

The measured data show a clear semi-diurnal pattern, with tidal ranges that oscillate between approximately 0.4 and 0.8 m between neap and spring tides at both locations, and Takaroa showing slightly

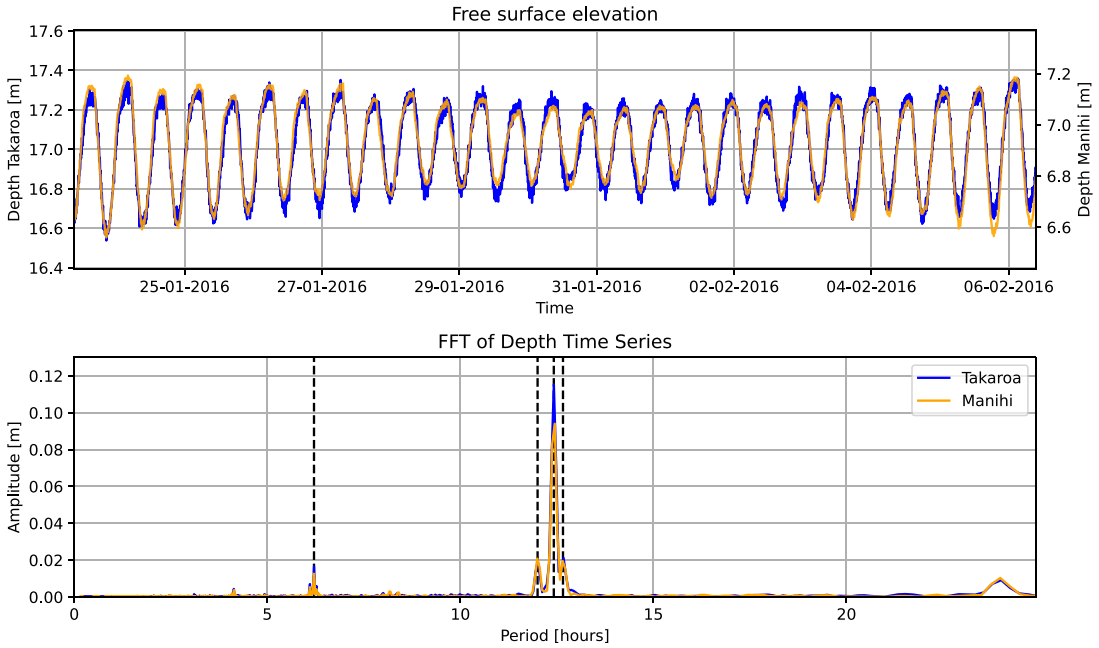

Fig. 6. Time series of free surface elevation over a sample period of 14 days at both Takaroa and Manihi (top) and Fast Fourier Transform of tidal elevation. The dashed vertical lines mark, from left to right, the M4, S2, M2, and N4 tidal periods.

higher amplitudes than Manihi. The FFTs clearly show a strong preponderance of the first lunar component M2, with a period of 12.421 h, followed by the main solar component S2 with a period of 12.000 h, the larger lunar elliptic semi-diurnal N2 with a period of 12.658 h, and the first lunar harmonic M4 with a period of 6.211 h.

While not negligible, the tidal ranges in both atolls are small compared to, e.g., those observed in sites of interest for the development of large-scale tidal stream energy. These include places such as the Bay of Fundy in Canada or the Severn Estuary in the UK, with mean ranges in order of 12.4 and 7.0 m, respectively [25]. However, as it was previously mentioned, a small tidal range does not necessarily correlate with slow currents. This is shown by the data collected in both atolls and shown in the following sections.

3.2. Velocity measurements

Fig. 7 shows contours of current speeds measured in Takaroa and Manihi as functions of depth and time, across the entire campaign. The figure marks the beginning and the end of each measurement period with black dashed lines as described in Table 1. The measurements show significant speeds, with upper layer maxima reaching ca. 3.4 m/s and 1.75 m/s for Manihi and Takaroa, respectively. The insets magnifying the data show 24 h of a typical day, from 15-05-2016 at 14:13:57. The insets highlight a semi diurnal pattern in both sites with the presence of some shear effects.

Note that white areas within the contours correspond to times and depths where ADCP data were not available. This includes the gap in the Manihi campaign, and it also includes the upper layers of the water column at both sites. Manihi shows no data in low tide conditions above 6 metres above the seabed, which agrees with the tidal elevation records and is consistent throughout the entire campaign. Takaroa shows differences in data availability over different periods. The first and second measurement windows show full data availability up to a bin located at 15.72 m from the seabed, which is consistent with the tidal elevation measurements. In the third and fourth periods this is reduced to the 13.72 and 12.72 m bins, respectively. No modifications to sensor deployment location, depth, or other differences have been recollected in the campaign logs. The blank bins have not been considered in the subsequent analysis.

3.2.1. Harmonic analysis

The FFTs of current speeds, presented in Fig. 8 for different depths d, measured from the seabed and at both sites, reflect the same harmonics as the tidal elevation FFT. This suggests a strong tidal influence driving the currents, with a dominance of both the lunar and solar constituents. The speed FFTs are dominated by the main lunar component M2, followed by the solar S2, and lunar M4, all with considerably lower amplitudes than M2.

Although both sites are relatively close to an amphidromic point and experience low tidal ranges, the velocity records still exhibit dominant lunar influence. Local bathymetry, tidal interactions and other phenomena such as wave overtopping, as will be shown later, can further amplify the otherwise weak regional tides, producing the strong currents observed.

3.2.2. Flow velocity directions and vertical profiles

Fig. 9 presents polar plots of current velocity for both sites and at different depths. The plots show that current directions are independent of depth. The channels present a relatively homogeneous bathymetry, with a seabed composed of sand and coral residuals, and without any relevant topographic features that could affect the flow.

In Takaroa, as expected, currents are relatively well aligned with the channel direction. The flood current shows a mean angle of approximately 80° to the north, while the ebb current is oriented at a mean angle of approximately 260°. Maxima for both ebb and flood tides are, as seen in the time series, in the order of 1.75 m/s. As with the current speeds, no significant seasonal effects were observed in the data.

Manihi currents are also well aligned with the channel. The flood current has a mean orientation angle of approximately 19° and maximum speeds in the order of 1.5 m/s, while the ebb currents have mean direction of 196°. The maximum speed is approximately 3.5 m/s.

The minor deviations in mean directions relative to the channel, as well as between ebb and flood tides, are attributed to the placement location of the ADCPs and local bathymetry.

Variations of current speed across the water column are presented in Fig. 10. The plots show time-averaged and fluctuations in the velocity profiles during the first trimester of measurements. The data shown is limited to this period due to a lower availability of upper layer

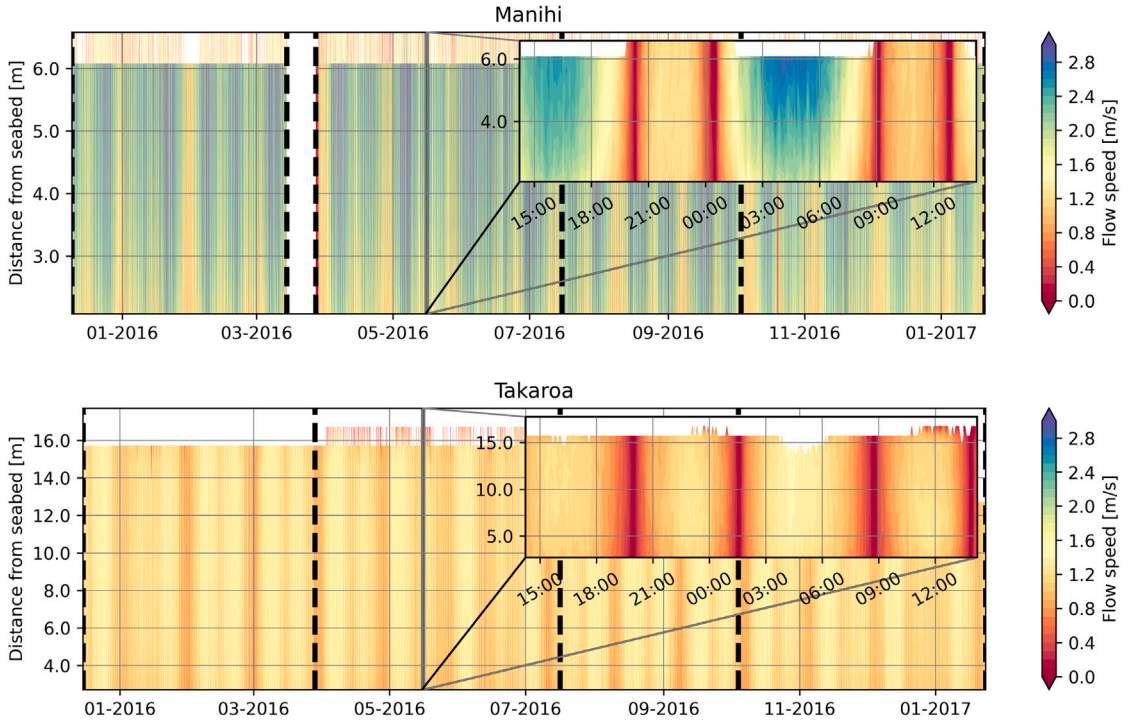

Fig. 7. Contours of velocity magnitude in Manihi and Takaroa as functions of time and depth. Depth is measured from the seabed. Blacked dashed lines mark the deployment and recovery of the instruments.

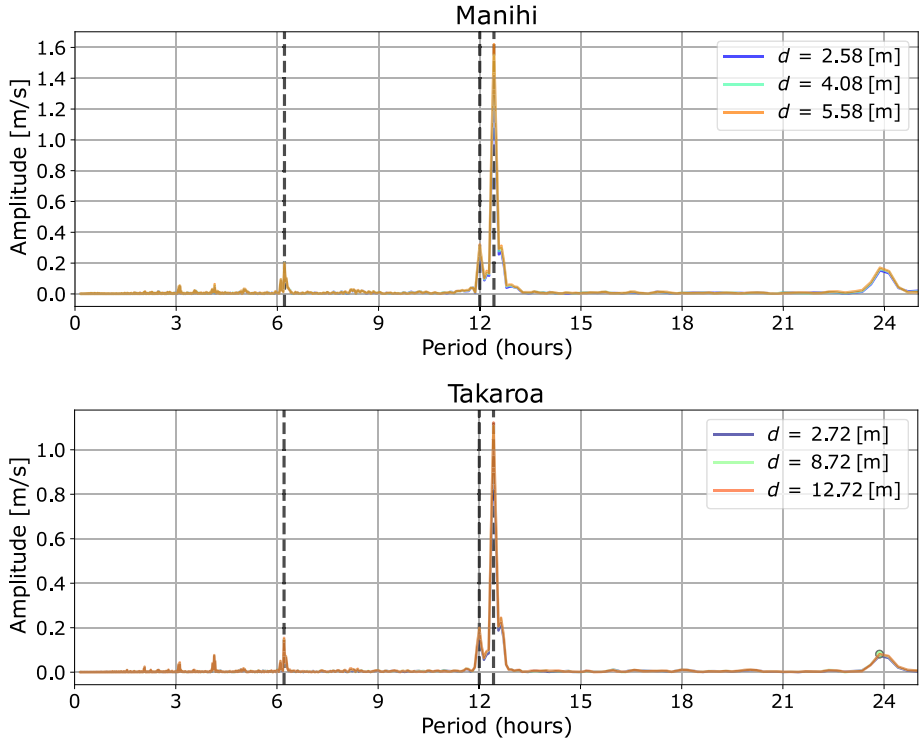

Fig. 8. Fast Fourier Transforms of flow speed calculated for Manihi and Takaroa at different depths d measured from the seabed. The dashed vertical lines mark the main solar (S2) and lunar (M2) periods at 12.00 and 12.42 h, respectively, as well as the main lunar harmonic (M4) at 6.21 h.

measurements in subsequent periods. While the data in the figure are limited, we did not observe significant deviations, seasonal or otherwise, in the rest of the available data. Flood and ebb tides have been separated based on the current direction, with positive and negative values corresponding to ebb and flood tides respectively.

The vertical profiles show that the mean speed in Takaroa, measured at the upper layers of the water column, has a value of ca. 0.95 m/s and 1.0 m/s for the flood and ebb tides, respectively, with a nearly symmetric behaviour. Manihi, on the contrary, shows faster currents than Takaroa, and a stronger asymmetry between flood and

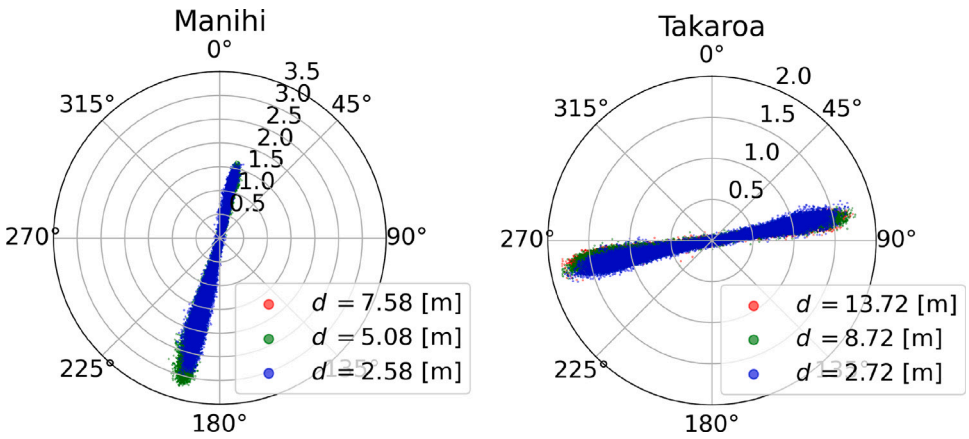

Fig. 9. Polar plots showing current speed and direction at different depths d relative to seabed. Data are presented for the first period of the measurement campaign.

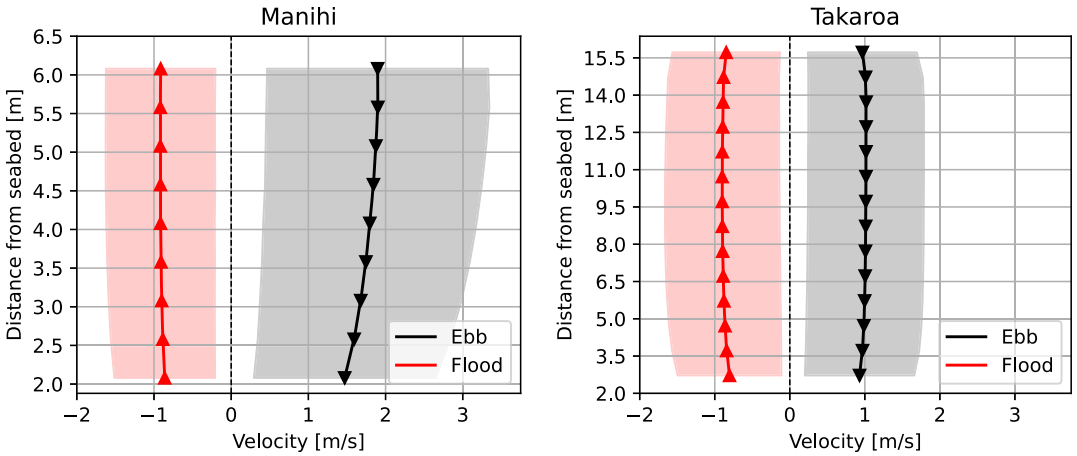

Fig. 10. Velocity profiles for ebb and flood tides. The markers and continuous lines correspond to the time-averaged profiles, while the shaded regions show the variation ranges from the mean represented by two standard deviations. Data processed from the first trimester of measurements.

ebb tides. Time-averaged speeds on the upper layers are ca. 0.95 m/s and 1.95 m/s for flood and ebb tides, respectively.

Except for the ebb velocity profile at Manihi, the remaining three cases show limited shear, which are only evident at the lower portion of the water column. The ebb tide in Manihi not only shows considerably faster speeds compared to the flood tide but also stronger velocity gradients, with the time-averaged profile showing a shear layer spanning through most of the depth of the channel.

Velocity fluctuation ranges are shown in Fig. 10 by two standard deviations from the mean, presented as shaded areas in the plots. The use of standard deviations instead of maxima and minima intends to provide representative ranges at different depths without strong outlier influence. In this figure, Takaroa shows only minor asymmetries in velocity fluctuations between both tides, with maximum speeds reaching up to approximately 1.8 m/s. As with the time-averaged speeds, Manihi shows a substantial asymmetry in speed fluctuations, with ebb tides reaching speeds above 3.0 m/s while the flood tide shows maxima below 1.8 m/s.

3.3. Impact of waves on flow velocities

Fig. 11 shows velocity time series at both sites during part of the campaign. The velocities are projected onto the mean direction of the flow, separating the ebb and flood tides in positive and negative values, respectively. Data are shown for a single depth (4.58 m and 8.72 m from the bottom at Manihi and Takaroa, respectively), but trends are representative of the entire water column.

As previously discussed, the plots show that the flood and ebb current speeds are approximately symmetrical in Takaroa, showing slightly faster currents during ebb, but with maxima and minima respectively above and below ±1.5 m/s. On the contrary, at Manihi, flow speeds are skewed, with maximum speeds during flood of approximately 1.5 m/s, and above 3.0 m/s during the ebb in spring tide.

Rolling averages presented for the two sites, computed with a 24-hour window, show positive non-zero values, a skew which suggests that the mass outflux during the ebb tide is larger than the influx in flood. The time segments highlighted with grey shades in the figure show periods where the rolling-averaged speed increases significantly and during which diminished flood currents and peak daily-averaged speeds are observed. This phenomenon is locally known as *ensachage*, which can be translated as bagging, and it is associated with wave overtopping. The phenomenon is typically observed occurring simultaneously at both atolls, as shown in Fig. 11.

Takaroa and Manihi are atolls that have only one significant channel connecting the lagoon to the outer ocean. The atoll boundaries, however, are low and may allow the passage of waves of a certain height. This wave overtopping mechanism provides for an external inflow of water into the lagoon that is at least partially discharged through the channel.

The highlighted data show periods where the instantaneous velocity does not become negative at Manihi for several days (i.e., the *ensachage* is strong enough to avoid any water influx through the channel). However, across the entire times series presented in Fig. 11, the non-zero mean values suggest that the *ensachage* phenomenon occurs

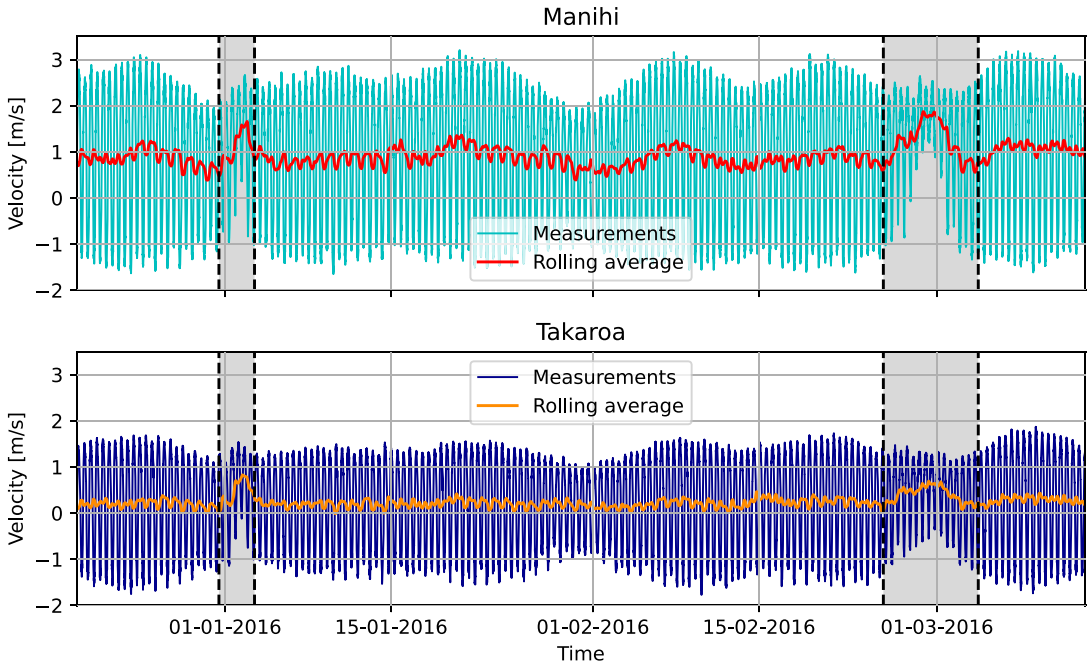

Fig. 11. Time series of velocity magnitude in Manihi and Takaroa identifying periods of *"ensachage"*.

permanently with different levels of intensity. An average flow speed of approximately 0.9 m/s is frequently encountered at Manihi and a lower value of approximately 0.2 m/s is observable in Takaroa.

Fig. 12 compares two segments of measurements taken over a two-day period at both sites. The first column corresponds to normal time where the rolling-averaged speeds remain close to the mean, while the second column shows a segment of the *ensachage* period previously highlighted in Fig. 11 on the right side of the plot. Maximum flow speeds show no substantial differences between the normal periods and those with *ensachage*. However, speed and direction plots highlight that even during normal times the duration of ebb and flood currents are different, with both sites showing a shorter influx of water through the channels. During the *ensachage* period at Manihi, data show a complete absence of flood currents, a pattern which indicates a substantial overtopping into the lagoon. Wave overtopping, however, does not remove the tidal influence, which is still evident in the figures in the form of periodic speed oscillations.

Records of wave height support the observations above. Fig. 13 shows a time series of significant wave height and direction, obtained from a reanalysis model [26] performed by Meteolien and Meteo-France. Data were extracted at a point located between the two islands at [14 °27.540' S; 145 °33.849' W; WGS84]. The significant wave height is presented alongside the rolling average of current speeds shown previously in Fig. 11.

Significant wave heights show a good correlation between currents and waves, especially during the strong *ensachage* periods highlighted in the plots. These periods also show predominant wave directions from the North-Northwest, reaching the atolls over their margins with largest exposure (see Figs. 2 and 3), presumably maximising wave overtopping. While the qualitative trends are similar, both atolls show different flow speeds. Despite their physical similarity, the edges of the atolls have different levels of permeability and have differences in channel cross sectional area (Fig. 4). Manihi's channel area, approximately 45% smaller than Takaroa's channel, is likely to propitiate faster currents under similar levels of wave overtopping.

A combination of large significant wave heights along with predominant wave directions from the north-northwest seem necessary to observe significant *ensachage* events such as those highlighted in Fig. 11. Regular significant wave heights of approximately $H_S = 2$ m seems to be sufficient to have positive 24-hours rolling averaged speeds both in Manihi and Takaroa, even if the speeds are much lower for the later.

Table 2
Energy consumption at the analysed atolls. SDE stands for *Service De l'Energie* and SIVMTG for *Syndicat Intercommunal à Vocation Multiple des Tuamotu-Gambier*.

Takaroa atoll		Source
Electricity consumption in 2019	277,104 kWh	SDE
Average daily consumption in 2019	759 kWh	calculated
Electricity consumption in 2022	355,549 kWh	SIVMTG
Average daily consumption in 2022	974 kWh	calculated
Manihi atoll		**Source**
Electricity consumption in 2019	582,938 kWh	SDE
Average daily consumption in 2019	1597 kWh	calculated
Electricity consumption in 2022	460,362 kWh	SIVMTG
Average daily consumption in 2022	1261 kWh	calculated

4. Energetic potential

4.1. Electricity consumption

Table 2 presents estimations of energy consumption in Manihi and Takaroa. The 2019 data correspond to estimates based on diesel consumption compiled by the *Service De l'Èenergie* (SDE), a governmental service of French Polynesia, while 2022 data correspond to measured domestic consumption without communal services such as municipal infrastructure and public lighting. The latter was provided by the *Syndicat Intercommunal à Vocation Multiple des Tuamotu-Gambier* (SIVMTG).[1] Daily consumption was calculated from available data and assumed constant through the year, an assumption supported by the region's limited seasonal weather variations. Nevertheless, energy consumption can vary significantly from year to year due to, e.g., installation or closure of tourist infrastructure.

[1] Private communication with the Technical Department of the SIVMTG, 2023.

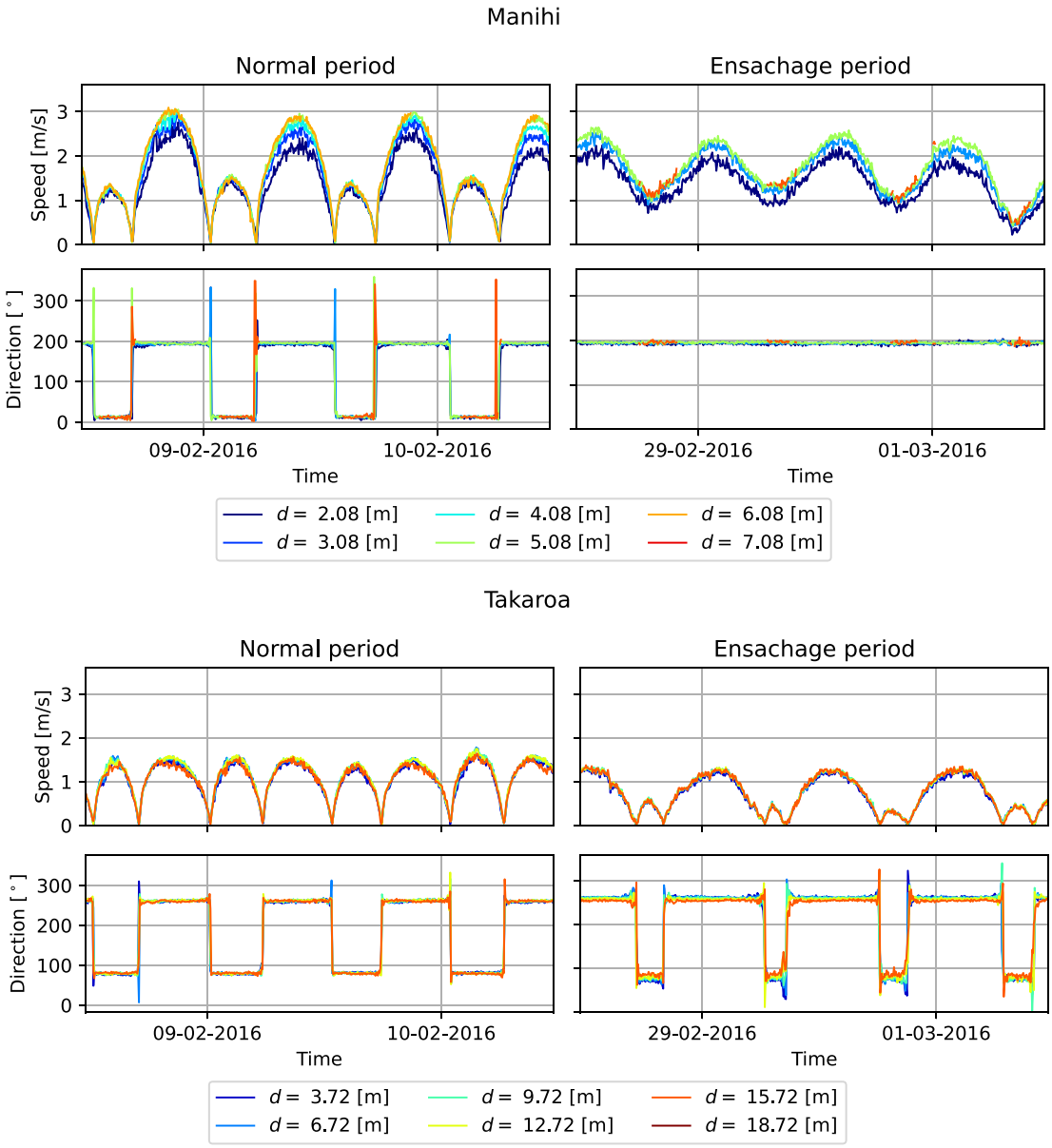

Fig. 12. Speed and direction comparison, at different depths d relative to seabed, between normal and *ensachage* period, both for Manihi (top) and Takaroa (bottom).

Electricity has a high price in French Polynesia. The consumer price was 268 €/MWh in Tahiti and other major islands in 2023 [27]. The cost of energy production, however, varies across the archipelagos, with an average cost in the order of 400 €/MWh [27]. In the Marquises, however, islands located further away from Tahiti, energy production can reach a cost of up to 1000 €/MWh [27]. These elevated figures are associated with oil prices, required logistics, and relatively low volumes of energy demand which impedes economies of scale.

Takaroa produces 100% of its electricity using diesel-powered generators, while Manihi has a solar installation capable of supplying up to 1250 kWh per day. While this solar production is substantial compared to demand, the intermittency of the resource means the population still relies on diesel generators as their baseline power supply. The energy demand in the islands is expected to grow alongside economic activity and transport electrification, suggesting that a robust and diverse energy mix is highly desirable even for islands with modest consumption and alternative power production arrangements [28,29].

4.2. Hydrokinetic energy potential

This section presents a parametric analysis to provide preliminary data on the potential benefits of various axial-flow tidal rotor configurations in both Manihi and Takaroa. Rotor radius and rated power were varied to assess hydrokinetic power production in both atolls using the *in situ* flow measurements. Power curves for generic turbines were defined with rated powers between 1 and 70 kW, and with diameters D ranging from 1 to 7 metres. The calculated power is then compared to local consumption.

The instantaneous power P generated by a tidal turbine is defined as:

$$P = \frac{1}{2}\rho A V^3 C_P, \tag{1}$$

where ρ is the sea water density ($\rho = 1025$ kg/m^3), A the rotor swept area ($A = \pi D^2/4$, with D the rotor diameter), V the flow speed, and C_P the non-dimensional power coefficient. Typical maximum power coefficients for well optimised 3-bladed horizontal axis rotors are typically between 0.35 and 0.45, although higher power coefficients

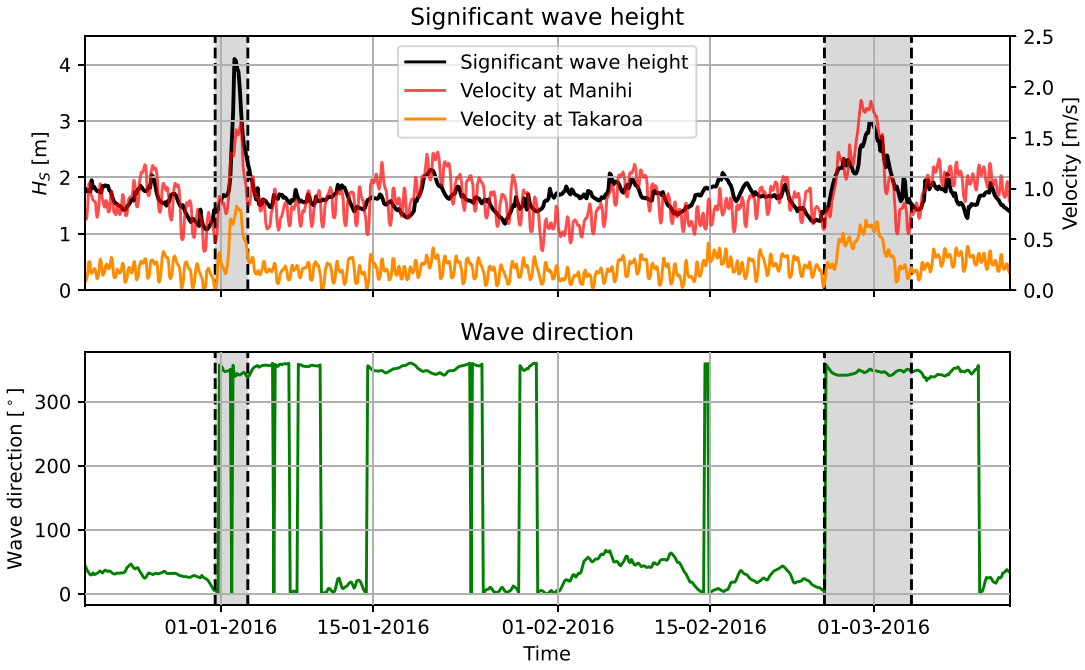

Fig. 13. Comparison of 24-hour rolling averaged velocity measured at both sites with significant wave height and wave direction obtained for a location in between the two islands. The periods shaded in grey indicate two events of strong *ensachage*.

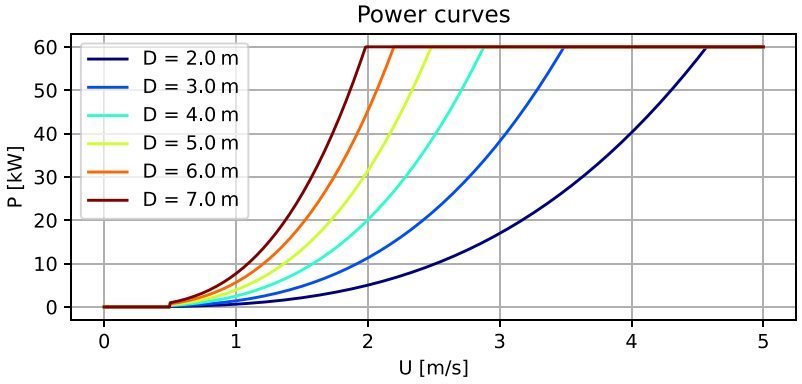

Fig. 14. Power curve of different synthetic turbines with a rated power $P_{rated} = 60\,\text{kW}$ and a pre-rated power coefficient of $C_P = 0.4$.

are achievable by exploiting blockage and local interference effects [30, 31].

The power curves for generic rotors were modelled by parametrically defining power curves as functions of flow speed, rated power, and diameter, following Eq. (1). The rated flow speed is, thus, dependent on rated power and diameter, and is defined as the minimum flow speed at which rated power is achieved with the rotor operating at maximum efficiency.

Each parametric power curve was divided into three regions of operation: a pre-cut-in speed region, for flow speeds below 0.5 m/s where $C_P = 0$; the pre-rated region where the turbine extracts power at maximum efficiency between cut-in and rated flow speed ($C_P = C_{P,max} = 0.40$); and the post-rated region where the power extraction is capped to rated power. Considering the moderate maximum speeds in both sites, no cut-out speed was considered. An example of six power curves, for turbines of different diameters with a rated power of 60 kW is shown in Fig. 14.

Yearly energy yields were computed using the modelled power curves, for the different combinations of rated power and rotor diameter, along with the available ADCP data of current speeds (Fig. 7). Energy yields are shown in the form of mean capacity factors (ratio of time-averaged generated power to rated power) in Table 3 and in Fig. 15. The figure also includes markers that depict the rated power and diameter of the commercial rotors shown in Table 4. The capacity factors show that Manihi has a much larger hydrokinetic potential than Takaroa due to the faster currents observed. The commercial rotors included in the figure, were they to be deployed at Manihi, could be expected to operate at capacity factors between 20 and 42%, or 5 to 11% at Takaroa.

Fig. 16 shows the average percentage of domestic power demands (taken as the mean between the 2019 and 2022 data in Table 2) that could be covered by exploiting the currents at Manihi and Takaroa with a single rotor. The figure shows that even a relatively small tidal stream rotor could contribute a substantial portion of the energy needs of Manihi. A larger rotor, such as the 6.3-metre SIT6.3, could provide power equivalent to approximately 80% of their estimated power demands, although the installation of such a device may not be technically feasible mainly due to the depth constraint (6.5 metres at the ADCP location). The 4-metre SIT4 counterpart, however, could be considered with a production slightly above 40% of estimated electricity demand.

Takaroa, despite showing less promising figures in terms of power production, has a much larger channel that could accommodate larger rotors deployed in arrays, while bespoke turbine designs suitable for low-speed conditions (i.e., rotors of large diameter and low rated

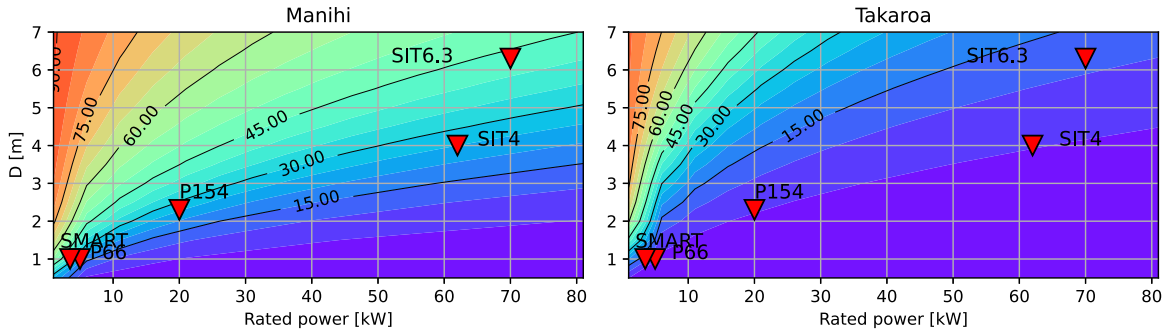

Fig. 15. Mean capacity factors as a function of rated power and diameter. Commercial turbines are included for reference (Table 4).

Table 3
Capacity factors for different rotor diameters D and rated powers at Manihi (left) and Takaroa (right).

Manihi							
D [m]	Rated power [kW]						
	1	20	30	40	50	60	70
2	0.7640	0.1954	0.1303	0.0977	0.0782	0.0652	0.0558
3	0.8484	0.3834	0.2857	0.2195	0.1759	0.1466	0.1257
4	0.8817	0.5012	0.4215	0.3555	0.3014	0.2577	0.2229
5	0.8975	0.5769	0.5085	0.4545	0.4074	0.3652	0.3281
6	0.9049	0.6374	0.5702	0.5219	0.4819	0.4462	0.4136
7	0.9072	0.6893	0.6211	0.5736	0.5365	0.5049	0.4766

Takaroa							
D [m]	Rated power [kW]						
	1	20	30	40	50	60	70
2	0.6079	0.0404	0.0269	0.0202	0.0162	0.0135	0.0115
3	0.7621	0.0909	0.0606	0.0454	0.0363	0.0303	0.0260
4	0.8193	0.1615	0.1077	0.0808	0.0646	0.0538	0.0462
5	0.8453	0.2523	0.1683	0.1262	0.1010	0.0841	0.0721
6	0.8573	0.3569	0.2422	0.1817	0.1454	0.1211	0.1038
7	0.8613	0.4579	0.3268	0.2472	0.1979	0.1649	0.1413

Table 4
Characteristics of axial-flow tidal turbines available in the market.

	SCHOTTEL Instream Turbine (SIT)		SMART Monofloat	Hydrolienne POSEIDE	
	SIT6.3	SIT4		P154	P66
Rated power [kW]	70	62	5	20	3.5
Rotor diameter D [m]	6.3	4.0	1.0	2.3	1.0
Rotor blades	3	3	3	3	3
Company	Schottel Hydro	Schottel Hydro	Smart Hydro Power	Guinard Energies Nouvelles	Guinard Energies Nouvelles
Country	Germany	Germany	Germany	France	France

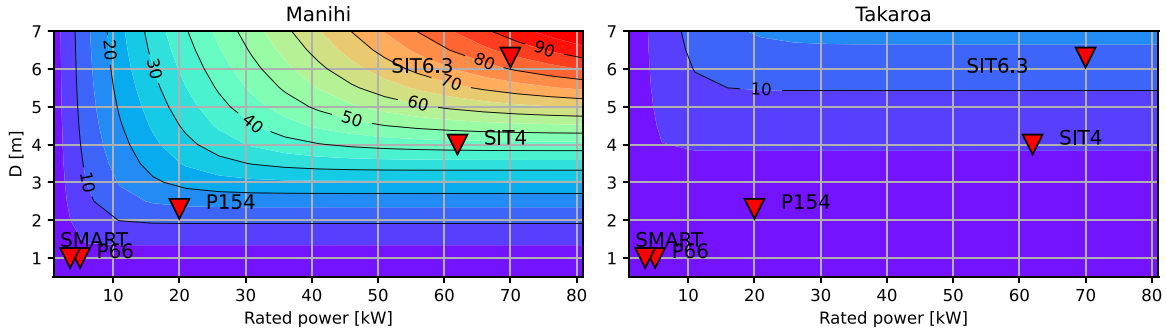

Fig. 16. Average percentage of power consumption supplied by a single turbine as a function of rated power and diameter. Commercial turbines are included for reference (Table 4).

power) could increase capacity factors and energy yields. The Teauonae pass in Takaroa is long, large and deep enough to possibly accommodate several tidal turbines [32,33], although larger deployments should consider the impact of added thrust in the channel flow [34].

The resource characterised in this study also offers advantages of robustness and predictability. In the case of a microgrid that relies on diesel or a combination with wind and solar, these advantages can enable substantial reductions in fossil fuel consumption, generator runtime [35], and energy storage requirements [29].

5. Conclusion

The data analysed in this paper shows that both Manihi and Takaroa, two atolls in French Polynesia, have a strong hydrokinetic energy potential. Our measurements show strong currents across the main channels that connect their internal lagoons with the outer ocean. These currents are dominated by lunar harmonics, despite French Polynesia being in an amphidromic region where the amplitude of the lunar tidal constituents is low.

The currents in these atolls, however, are not only driven by tides. The measured data show differences in the temporal length between ebb and flood currents, as well as non-zero daily-averaged flow speeds, with generally longer ebb periods. This implies that the mass outflux through the channel during the ebb tide is larger than the influx during flood. The phenomenon is increased during periods of *ensachage*, with records showing several days when Manihi would not have water flooding the lagoon through its main channel. Comparison with significant wave heights from a reanalysis model shows a strong correlation

with daily-averaged measured flow speeds, especially during strong *ensachage* periods. This evidence suggests that atolls operate as wave overtopping devices, with waves regularly permeating the low coral barriers and providing an influx of seawater to the lagoon.

A simple analysis of power production in both sites shows promising results. The approach taken has limitations as we have not considered asymmetric performance coefficients for ebb and flood currents, blockage, multi-rotor interactions, or flow choking due to increased thrust in the channel. The latter, in particular, should be studied in more detail given the permeability of the barrier supporting head differences between the atoll and the sea. Nevertheless, power curve estimations are conservative and the analysis has been limited to a single rotor rather than turbine arrays, suggesting a reduced impact on channel dynamics. We conclude, thus, that the analysis is valid as a first estimation of energetic potential.

Manihi, in particular, is a promising site for an initial deployment of hydrokinetic turbines. Large capacity factors with a relatively low demand for electricity indicate that even a small rotor could supply a significant proportion of the atoll's energy needs. The combination of a robust and predictable supply of tidal stream energy with an existing solar installation, in addition to low-capacity energy storage, could potentially drive a further penetration of renewables and a displacement of fossil fuels. An energy mix based 100% on locally-produced renewables for an atoll in French Polynesia not only would enforce energy security but could also act as a flagship project for further installations, both in this region as well as for other isolated communities worldwide.

Takaroa exhibited significantly lower speeds and energy yields compared to Manihi. Its channel, however is considerably larger in length and cross sectional area. It could potentially accommodate more rotors of larger capacity, which we speculate could supply a significant portion of the atoll's energy needs. Such a deployment, however, would increase channel thrust significantly, requiring consideration of channel dynamics and potential choking effects.

CRediT authorship contribution statement

Federico Zilic de Arcos: Writing – review & editing, Writing – original draft, Visualization, Software, Methodology, Investigation, Formal analysis, Data curation, Conceptualisation. **Minh Anh Pham:** Formal analysis. **Franck Lucas:** Methodology, Investigation, Funding acquisition. **Marc Lafosse:** Methodology, Investigation, Data curation. **Grégory Pinon:** Writing – review & editing, Writing – original draft, Resources, Project administration, Methodology, Investigation, Formal analysis, Conceptualisation.

Declaration of competing interest

The authors declare the following financial interests/personal relationships which may be considered as potential competing interests: Federico Zilic de Arcos reports financial support was provided by Horizon Europe. Other authors declare that they have no known competing financial interests or personal relationships that could have appeared to influence the work reported in this paper.

Acknowledgements

GP would like to acknowledge the DEFIER initiative for initiating this work and organising the workshop in Dec. 2022. The authors would like to acknowledge the support received from Dr. Tea Frogier, and from the newly created GdR CNRS TranPolyn. The authors would also like to thank the governmental *Service de l'Energie of French Polynesia* and Thomas Biarez from the *Syndicat Intercommunal à Vocation Multiple des Tuamotu-Gambier* for providing energy consumption data in Manihi and Takaroa. The authors would like to thank Hélène Chabbert from Meteolien, Corinne Dubois from YS Energies Marines Developpement SAS and Meteo-France for providing wave data. FZdA acknowledges the support from the European Union's Horizon 2020 research and innovation programme under the Marie Skłodowska-Curie grant agreement No. 101034329 and the WINNINGNormandy programme supported by the Normandy Region.

References

[1] H. Lucas, S. Fifita, I. Talab, C. Marschel, L.F. Cabeza, Critical challenges and capacity building needs for renewable energy deployment in Pacific small island developing states (Pacific SIDS), Renew. Energy 107 (2017) 42–52, http://dx.doi.org/10.1016/j.renene.2017.01.029.

[2] J. Hourçourigaray, D. Wary, S. Bitot, Renewable Energy in the Pacific Islands: An Overview and Exemplary Projects, Technical Report, Agence Française de Développement (AFD), Paris, France, 2014, Coordination: Frédéric Audras (Papeete Agency) and Françoise Rivière (Research and, URL: https://prdrse4all.spc.int/sites/default/files/energies-renouv-va_0.pdf.

[3] International Renewable Energy Agency (IRENA), Energy profile: French polynesia, 2022, URL: https://www.irena.org/-/media/Files/IRENA/Agency/Statistics/Statistical_Profiles/Oceania/French%20Polynesia_Oceania_RE_SP.pdf. Last updated: 2022-08-24.

[4] Agence Française de Développement (AFD), Supporting French polynesia's energy transition, 2020, URL: https://www.afd.fr/en/carte-des-projets/supporting-french-polynesias-energy-transition. (Accessed 31 March 2023).

[5] Institut de la statistique de la Polynésie Française (ISPF), French Polynesia at a glance 2020, Retrieved 2022-03-04.

[6] J. Borges Posterari, T. Waseda, Wave energy in the Pacific island countries: A new integrative conceptual framework for potential challenges in harnessing wave energy, Energies 15 (7) (2022) http://dx.doi.org/10.3390/en15072606, URL: https://www.mdpi.com/1996-1073/15/7/2606.

[7] C. Bosserelle, J. Kruger, S. Reddy, Cost Analysis of Wave Energy in the Pacific, Technical Report, Waves and Coasts in the Pacific (WACOP), 2015.

[8] K. Sanjivy, O. Marc, N. Davies, F. Lucas, Energy performance assessment of sea water air conditioning (SWAC) as a solution toward net zero carbon emissions: A case study in French Polynesia, Energy Rep. 9 (2023) 437–446, http://dx.doi.org/10.1016/j.egyr.2022.11.201, URL: https://www.sciencedirect.com/science/article/pii/S2352484722025884.

[9] Meteolien, Tahiti wave energy challenge (TWEC), 2024, URL: https://www.meteolien.com/tahiti-wave-energy-challenge-twec/. (Accessed 31 March 2024).

[10] F. Sinama, M. Martins, A. Journoud, O. Marc, F. Lucas, Thermodynamic analysis and optimization of a 10MW OTEC rankine cycle in reunion island with the equivalent Gibbs system method and generic optimization program GenOpt, Appl. Ocean Res. 53 (2015) 54–66, http://dx.doi.org/10.1016/j.apor.2015.07.006.

[11] M.A. Almoghayer, D.K. Woolf, S. Kerr, G. Davies, Integration of tidal energy into an island energy system–a case study of Orkney islands, Energy 242 (2022) 122547.

[12] M. Lewis, R. Lowe, R. Green, M. Buckley, M. Hemer, J. Demmer, S. Neill, A novel marine renewable energy resource in coral reefs: Utilising the hydrokinetic energy of wave-induced currents, 2022, Ocean Sciences Meeting (OSM 2022), Education and Policy Session OP04 Marine Renewable Energy: Resource Characterization, Bio-physical Interactions, and Societal Impacts, Oral Presentation, URL: https://osm2022.secure-platform.com/a/gallery/rounds/3/details/924.

[13] International Electrotechnical Commission (IEC), IEC/TS 62600-201:2013 – marine energy – wave, tidal and other water current converters – part 201: Tidal energy resource assessment and characterization, 2015, Technical Specification, Geneva, Switzerland, Edition 1.0.

[14] B.G. Sellar, G. Wakelam, D.R. Sutherland, D.M. Ingram, V. Venugopal, Characterisation of tidal flows at the European Marine Energy Centre in the absence of ocean waves, Energies 11 (1) (2018) 176.

[15] R. Cossu, I. Penesis, J.-R. Nader, P. Marsh, L. Perez, C. Couzi, A. Grinham, P. Osman, Tidal energy site characterisation in a large tidal channel in Banks Strait, Tasmania, Australia, Renew. Energy 177 (2021) 859–870.

[16] S.P. Neill, I.A. Fairley, S. Rowlands, S. Young, T. Hill, C.A. Unsworth, N. King, M.J. Roberts, M.J. Austin, P. Hughes, et al., Characterizing the Marine Energy Test Area (META) in Wales, UK, Renew. Energy 205 (2023) 447–460.

[17] L. Evans, I. Ashton, B. Sellar, Tidal turbine power performance assessments following IEC TS 62600-200 using measured and modelled power outputs, Renew. Energy 212 (2023) 138–150.

[18] M. Lewis, S. Neill, P. Robins, M.R. Hashemi, S. Ward, Characteristics of the velocity profile at tidal-stream energy sites, Renew. Energy 114 (2017) 258–272.

[19] M. Guerra, R. Cienfuegos, J. Thomson, L. Suarez, Tidal energy resource characterization in Chacao Channel, Chile, Int. J. Mar. Energy 20 (2017) 1–16.

[20] L. Suarez, M. Guerra, M.E. Williams, C. Escauriaza, Tidal energy resource assessment in the Strait of Magellan in the Chilean Patagonia, Renew. Energy (2025) 123430.

[21] Z. Yang, T. Wang, R. Branch, Z. Xiao, M. Deb, Tidal stream energy resource characterization in the Salish Sea, Renew. Energy 172 (2021) 188–208.

[22] C. Giry, J. Cougoul, Étude de courantologie - Rapport de synthèse et préconisations, 2017, Rapport de synthése et préconisations, Energie de la Lune.
[23] NASA Scientific Visualization Studio, R. Ray, NASA Goddard Space Flight Center, Jet Propulsion Laboratory, TOPEX/Poseidon: revealing hidden tidal energy, 2019, https://svs.gsfc.nasa.gov/stories/topex/tides.html. (Accessed 12 June 2025).
[24] C. Giry, J. Cougoul, Étude de courantologie - Service des énergies, Polynésie Française – Campagne BMADCP trimestre 1, Manihi et Takaroa, 2016, Rapport intermédiaire, Energie de la Lune.
[25] S.P. Neill, A. Angeloudis, P.E. Robins, I. Walkington, S.L. Ward, I. Masters, M.J. Lewis, M. Piano, A. Avdis, M.D. Piggott, et al., Tidal range energy resource and optimization–past perspectives and future challenges, Renew. Energy 127 (2018) 763–778.
[26] Meteolien, Atlas de l'énergie des vagues de Polynésie Française, 2024, (Accessed 31 March 2024). URL: https://www.meteolien.com/atlas-de-lenergie-des-vagues-de-polynesie-francaise/.
[27] Service De l'Energie, Private communication with a member of the Service De l'Energie, French Polynesia, 2023.
[28] T.J. Vaiaso, M. Jack, Quantifying the trade-off between percentage of renewable supply and affordability in Pacific island countries: Case study of samoa, Renew. Sustain. Energy Rev. 150 (2021) 111468.
[29] F. Han, J. Zeng, J. Lin, C. Gao, Z. Ma, A novel two-layer nested optimization method for a zero-carbon island integrated energy system, incorporating tidal current power generation, Renew. Energy 218 (2023) 119381.
[30] C. Garrett, P. Cummins, The efficiency of a turbine in a tidal channel, J. Fluid Mech. 588 (2007) 243–251, http://dx.doi.org/10.1017/S0022112007007781.
[31] J. McNaughton, B. Cao, A. Nambiar, T. Davey, C.R. Vogel, R.H. Willden, Constructive interference effects for tidal turbine arrays, J. Fluid Mech. 943 (2022) A38, http://dx.doi.org/10.1017/jfm.2022.454.
[32] P. Mycek, B. Gaurier, G. Germain, G. Pinon, E. Rivoalen, Experimental study of the turbulence intensity effects on marine current turbines behaviour. Part II: Two interacting turbines, Renew. Energy 68 (2014) 876–892, http://dx.doi.org/10.1016/j.renene.2013.12.048.
[33] G. Pinon, M.F. Hurst, E. Lukeba, Semi-analytical estimate of energy production from a tidal turbine farm with the account of ambient turbulence, Int. J. Mar. Energy 19 (2017) 70–82, http://dx.doi.org/10.1016/j.ijome.2017.05.003.
[34] C. Garrett, P. Cummins, The power potential of tidal currents in channels, Proc. R. Soc. A: Math. Phys. Eng. Sci. 461 (2060) (2005) 2563–2572.
[35] P.B.L. Neto, O.R. Saavedra, D.Q. Oliveira, The effect of complementarity between solar, wind and tidal energy in isolated hybrid microgrids, Renew. Energy 147 (2020) 339–355.